Supporting Information

Achieving efficient and stable inorganic $CsSnI_3$ mesoporous perovskite solar cells *via* galvanic displacement reaction

Zhiguo *Zhang* [a, †], Qiang Sun [a, †], Takahito Nakajima [b], Huaxia Ban [a], Zhirong Liu [a], Huaixuan Yu [a], Yin Wang [c], Zewen Xiao [a], Yan Shen [a,*] and Mingkui Wang [a,d,*]

[a] Wuhan National Laboratory for Optoelectronics, Huazhong University of Science and Technology, 1037 Luoyu Road, Wuhan 430074, Hubei, P. R. China. E-mail: mingkui.wang@mail.hust.edu.cn

[b] RIKEN Center for Computational Science, 7-1-26 Minatojima-minami-machi, Chuo-ku, Kobe, Hyogo, Japan

[c] Hubei Key Laboratory of Low Dimensional Optoelectronic Materials and Devices, Hubei University of Arts and Science, Xiangyang, 441053, Hubei, P. R. China

[d] Optics Valley Laboratory, Hubei 430074, China

[+] These authors contributed equally to this work

[*]Corresponding author, E-mail: ciac_sheny@mail.hust.edu.cn (Y.S.), mingkui.wang@mail.hust.edu.cn (M. Wang)

Experimental Section

Materials: CsI (99.99%, Sigma Aldrich), SnI_2 (99.99%, Sigma Aldrich), ZnI_2 (99.99%, Sigma Aldrich), zinc powder (99.99%, Sigma Aldrich), N, N-Dimethylformamide (DMF, Anhydrous 99.8%, Sigma Aldrich), and dimethyl sulfoxide (DMSO, Anhydrous ≥99.5%, Sigma Aldrich) were used as received from commercial without further purified.

$CsSnI_3$ films fabrication: The films were fabricated on glasses in a N_2-filled glove box. The substrates were sequentially ultrasonically cleaned with detergent, water, deionized water, acetone and ethanol. Then, the substrates were treated by UV ozone for 30 min. The precursor solution was spin-coated on substrates at 3000 rpm for 30 s. Finally, the substrate was annealed at 60 ℃ for 5 min to finish the $CsSnI_3$ film fabrication.

PSC devices fabrication: For control perovskite precursor solution, CsI and SnI_2, with a molar ratio of 1: 1 were dissolved in the mixed solvent of DMF and DMSO (4:1 in volume ratio) to obtain 0.7 M/L solution. The GDR-based perovskite solution was prepared by mixing solid Zn powders into the prepared control perovskite solutions. Normally, the solution was kept and stirred at 50 ℃. For common-5ZnI_2 perovskite precursor solution, CsI, SnI_2, ZnI_2, with a molar ratio of 1:0.95:0.05 were dissolved in DMF and DMSO solvent with a total concentration of 0.7 M/L. Then a 2.5μL solution was dropped on the prepared all-inorganic FTO/c-TiO2/m-TiO_2/Al_2O_3/NiO/carbon mesoscopic framework. Finally, the devices were annealed at 70 ℃ for 15 min to finish the fabrication. All the fabrication steps were conducted in an Ar-filled glove box.

All-inorganic mesoscopic framework fabrication: All-inorganic mesoscopic framework was fabricated on fluorine doped tin oxide (FTO) coated glass used as transparent electrode and substrate, respectively. The etched FTO glass was sequentially ultrasonically cleaned with detergent, water, deionized water, and ethanol. Then, FTO was treated by UV ozone for 30 min. Subsequently, a 50 nm thick compact TiO_2 layer was deposited on the cleaned FTO substrate by spray pyrolysis deposition with titanium isopropoxide (trance metals basis, Aldrich) ethyl alcohol solution at 450 ℃, holding for 30 min. After the temperature dropped to 25 ℃, a 400 nm-thick mesoporous TiO_2 nanocrystal film (DSL 30NR-T, Dyesol, Australia, diluted with

terpinol, 1/3.5 mass ratio), a 450 nm-thick Al_2O_3 insulating layer (20 nm γ-Al_2O_3 nanoparticles, Aladdin), an 800 nm-thick NiO layer (30 nm sized nanoparticles, Inframat) were deposited with screen printing method onto FTO sequentially. Following heating the paste in the air flow with a procedure of 112°C for 5 min, 175℃ for 5 min, 350 ℃ for 10 min, 400 ℃ for 15 min, and 500 ℃ for 30 min. Then, a 20 μm carbon paste was printed on the top of the NiO layer as a counter electrode and sintered in the air at 400 ℃ for 30 min to finish the mesoscopic framework of FTO/c-TiO_2/m-TiO_2/Al_2O_3/NiO/Carbon.

Characterization: X-ray diffraction (XRD) experiments were conducted using a Philips X-ray diffractometer with Cu Kα radiation to measure the crystal structure. The film light absorption was measured with a PE950 spectrophotometer at room temperature. TEM and HRTEM measurement were carried out by Talos F200X. UV-Vis absorption spectra were observed with a PE950 spectrophotometer. The film morphology was obtained with a field-emission scanning electron microscope (FEI Nova Nano SEM 450). The steady-state photoluminescence (PL) spectrum was measured by a fluorescence spectrophotometer (LabRAM HR800). Inductively coupled plasma optical emission spectroscopy (ICP-OES) was measured using Prodigy Plus ICP-OES. X-ray photoelectron spectrometer (XPS) measurements were conducted on an AXIS SUPRA system (Kratos Analytical Ltd.). Time-resolved photoluminescence decays (TRPL) were measured at 820 nm with a 500 nm light pulse as excitation by Delta Flex Fluorescence Lifetime System (Horiba Scientific Com., Japan). The photocurrent density-voltage (J-V) characteristics of the devices were obtained by applying external potential bias to the devices and measuring the generated photocurrent with a Keithley model 2400 digital source meter. A xenon light source solar simulator (450 W, Oriel, model 9119) with AM 1.5G filter (Oriel, model 91192) was used to give an irradiance of 100 mW cm-2 at the surface of solar cells. All devices were measured using a metallic mask with an aperture area of 0.198 cm2. A similar data acquisition system was used to control the incident photon-to-current conversion efficiency (EQE) measurement. A white-light bias (10% sunlight intensity) was applied

onto the sample during the EQE measurements with the alternating current (AC) model (130 Hz). The electronic impedance (EIS) measurements were measured using the PGSTAT302N frequency analyzer from Autolab (The Netherlands), together with the frequency response analyzer module providing voltage modulation in the desired frequency range.

Computational details

DFT calculations: The first principles computations were carried out by Vienna Ab initio Simulation Package (VASP) based on density functional theory. Generalized gradient approximation (GGA) with the Perdew–Burke–Ernzerhof (PBE) functional was used to describe the exchange-correlation interaction. Based on the optimized black-γ-$CsSnI_3$ unit cell, a six-layer slab model ofγ-$CsSnI_3$ (202) surface was constructed. The bottom 4 layers were fixed at its original bulk position and the top 2 layers were fully relaxed for structure optimization. The vacuum slab was set as 15 Å for all models to eliminate the interaction between neighboring supercell. The projector augmented wave pseudopotentials were adopted to describe the ion-electron with a cutoff energy of 500eV. The K-point grid of Brillouin zone was tested and sampled by 2 ×2 ×1 within Gamma-Pack. The convergence criterion for electronic structure iteration and geometry optimizations were set to 10^{-5} eV $Å^{-1}$ and 10^{-3} eV $Å^{-1}$, respectively. For the O_2 adsorption calculation, the spin polarization correction was incorporated due to O_2 is the triplet ground stateits. In order to calculate the Mulliken charge, The Cambridge Sequential Total Energy Package (CASTEP) was employed in the first-principles calculations. The calculation was based on density functional theory using a plane-wave pseudopotential formalism, aided by the Accelrys Materials Studio (Accelrys Inc.) graphical front-end interface.

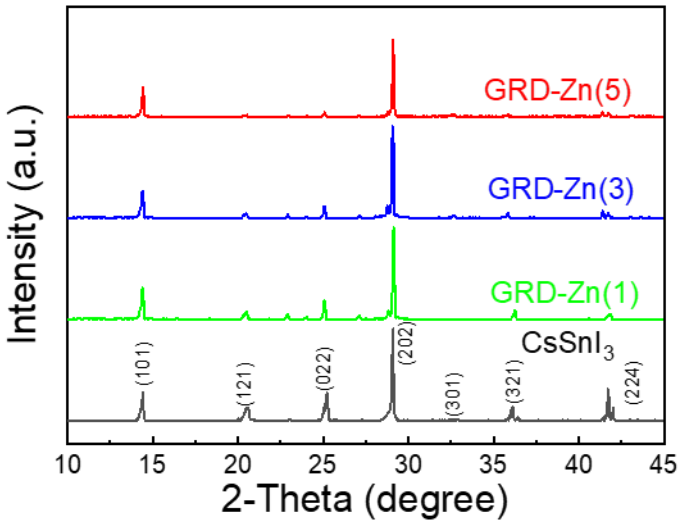

Figure S1. The XRD patterns of $CsSnI_3$ and GDR-Zn perovskite films.

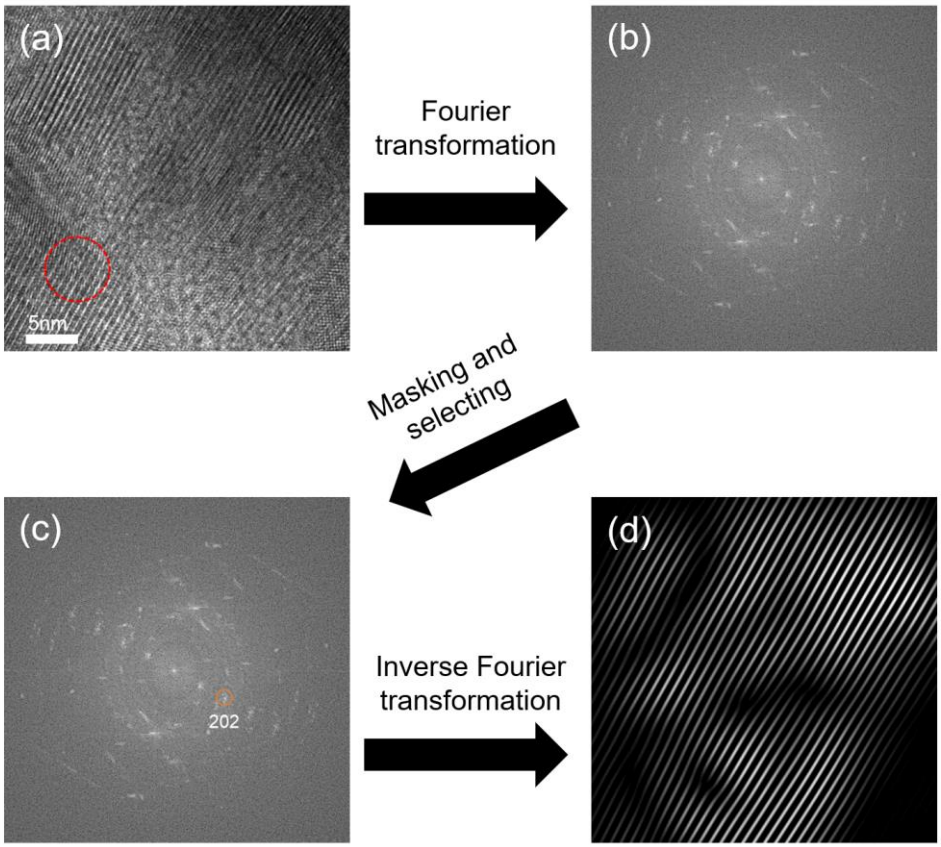

Figure S2. Procedure of the Fourier filtering and reconstruction technique; (a) the original TEM image, (b) FFTs from (a), (c) FFTs composed of specific diffraction spots masked and selected from (b) for image refinement, (d) refined TEM images reconstructed by inverse Fourier transformation with (c).

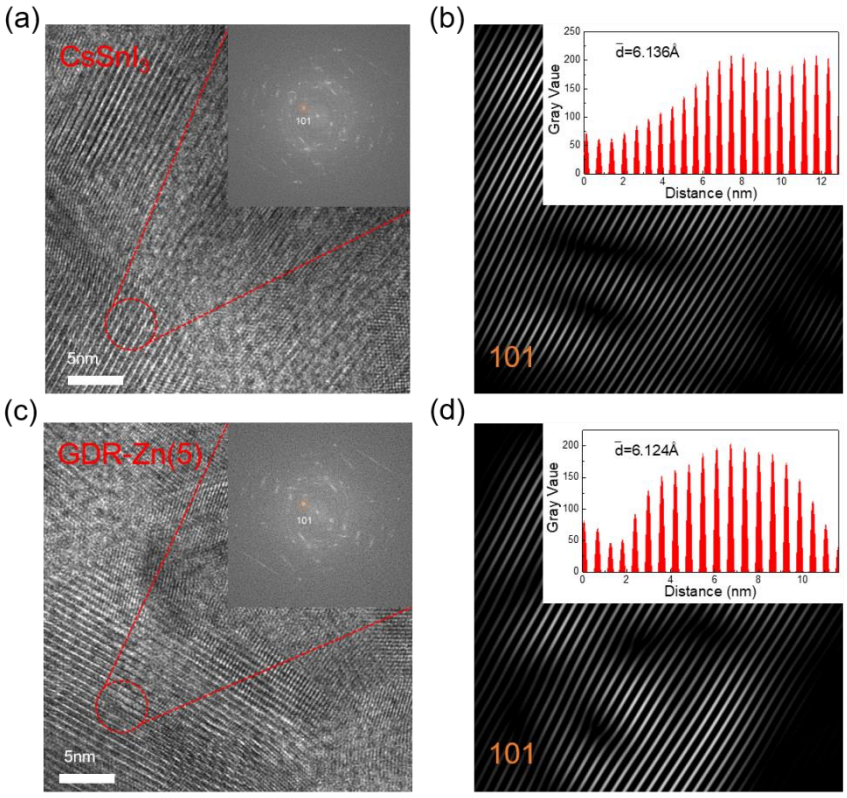

Figure S3. The TEM images of (a) $CsSnI_3$ films, (c) GDR-Zn (5) films (inset: the FFT pattern of the corresponding red circle part). Refined TEM images of (b) $CsSnI_3$, (d) GDR-Zn (5) (101) surface obtained through the Fourier filtering and reconstruction technique (inset: the intensity profiles recorded from the corresponding lines shown in panel).

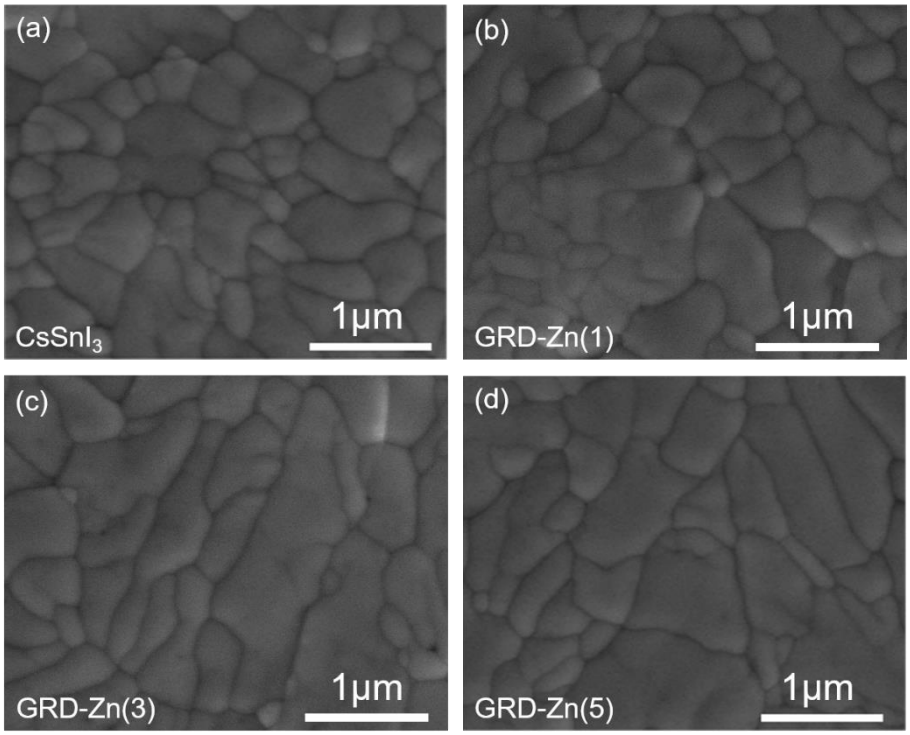

Figure S4. Top-view SEM images of (a) $CsSnI_3$ films, (b) GDR-Zn (1) films, (c) GDR-Zn (3) films, (d) GDR-Zn (5) films on ITO substrate.

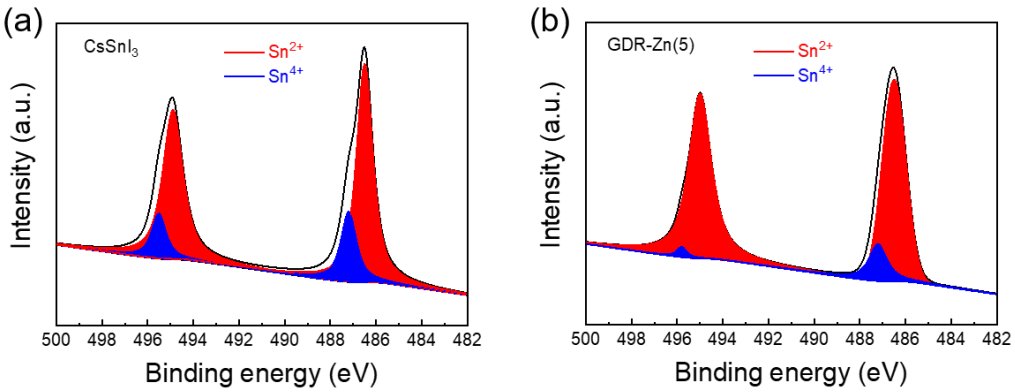

Figure S5. The Sn 3d bands XPS spectra of (a) control and (b) GDR-Zn (5) perovskite films.

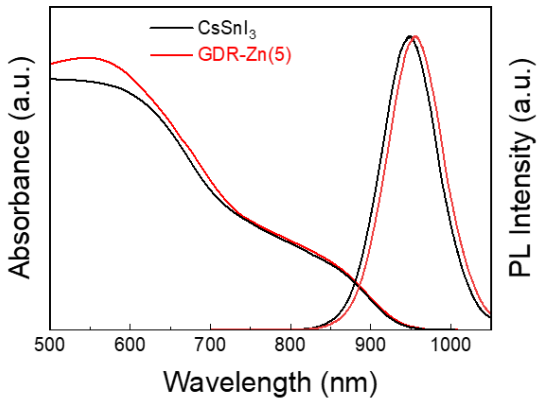

Figure S6. The UV-vis absorption spectroscopy and steady photoluminescence (PL) spectroscopy characterization for the $CsSnI_3$ and GDR-Zn (5) perovskite films.

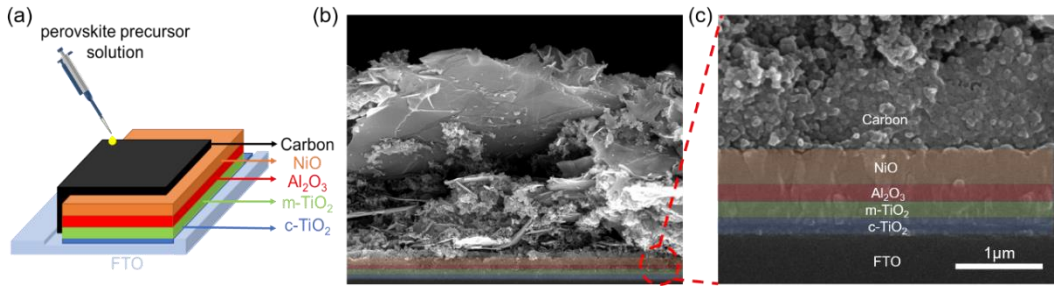

Figure S7. (a) Schematic representation of the $TiO_2/Al_2O_3/NiO$/carbon ($CsSnI_3$) based device. (b) Cross section SEM image of the device with $TiO_2/Al_2O_3/NiO$/carbon ($CsSnI_3$) structure. (c) large-view cross section SEM image of red frame in (a).

The devices were fabricated within a printable mesoscopic metal oxide framework of $TiO_2/Al_2O_3/NiO$/carbon counter electrode without sealing. In this device structure, each layer has been selected with its own purpose in this device structure. TiO_2 layer has been widely used as the ETL because of its high temperature resistance and efficient electron extraction capability. The Al_2O_3 layer is applied between the mesoporous TiO_2 (n-type) and NiO (p-type) layers to prevent the direct contact between these two semiconductors and to realize a P-I-N metal oxide framework configuration. The NiO layer can accelerate the hole extraction from perovskite material. The carbon counter electrode can greatly reduce the cost of precious metal electrode and be more conducive to commercialization.

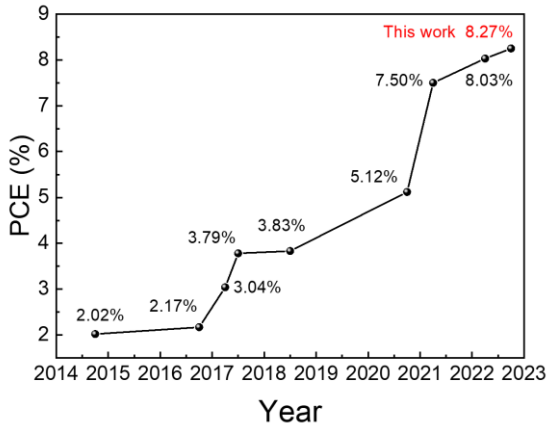

Figure S8. The efficiency progress of fully inorganic tin-based mesoporous solar cells over recent years. (2014,[1] 2016,[2] 2017,[3,4] 2018,[5] 2021,[6,7] 2022[8])

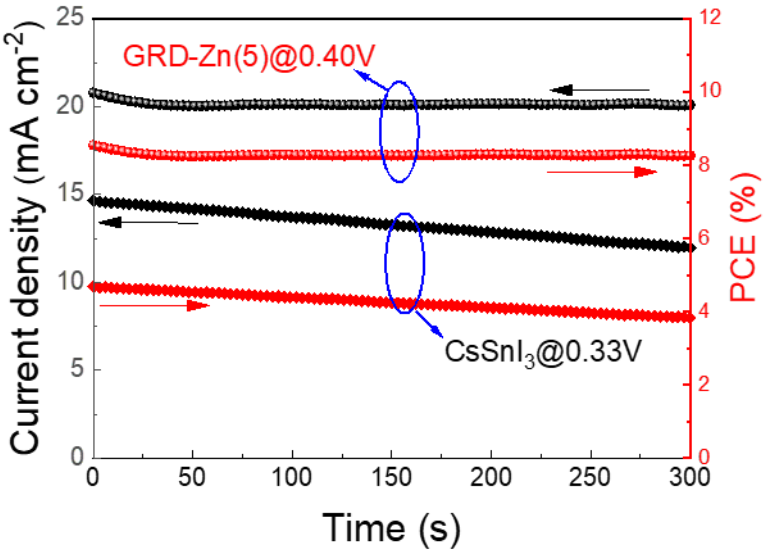

Figure S9. Steady-state photocurrent and power output of the GDR-Zn (5) and $CsSnI_3$-based PSC.

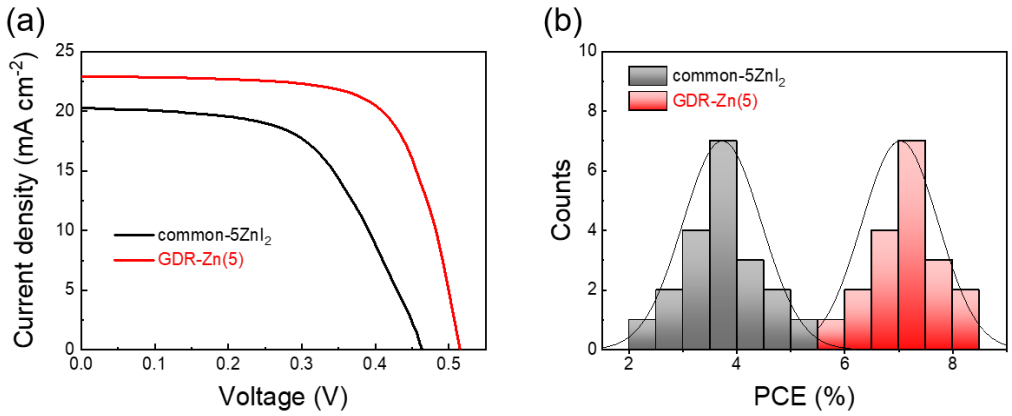

Figure S10. a) The *J-V* curves of the best-performing common-5ZnI_2 and GDR-Zn (5) solar cells. b) PCE histograms obtained from 20 individual common-5ZnI_2 perovskite solar cells and 20 individual GDR-Zn (5) perovskite solar cells.

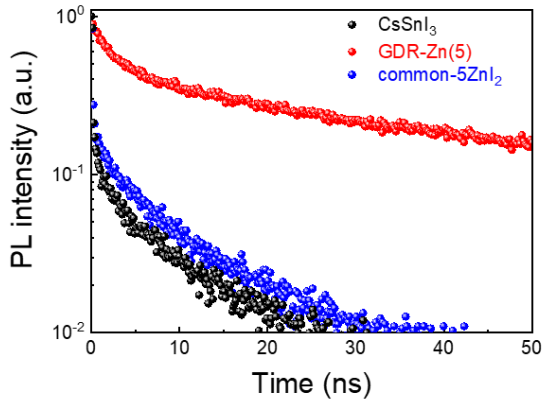

Figure S11. The time-resolved photoluminescence spectra (TRPL) of different perovskite films on glass.

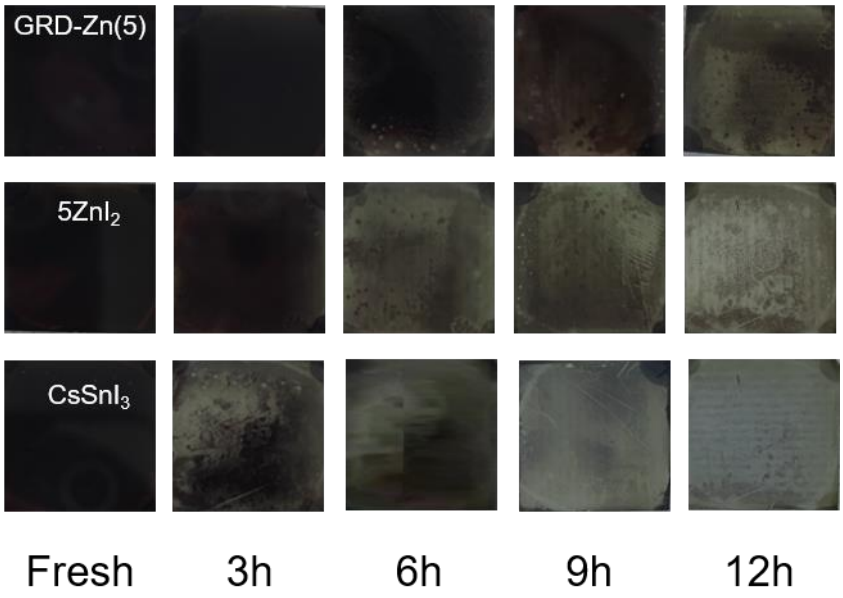

Figure S12. Photographs of the GDR-Zn (5), common-$5ZnI_2$ and $CsSnI_3$-based films based on time.

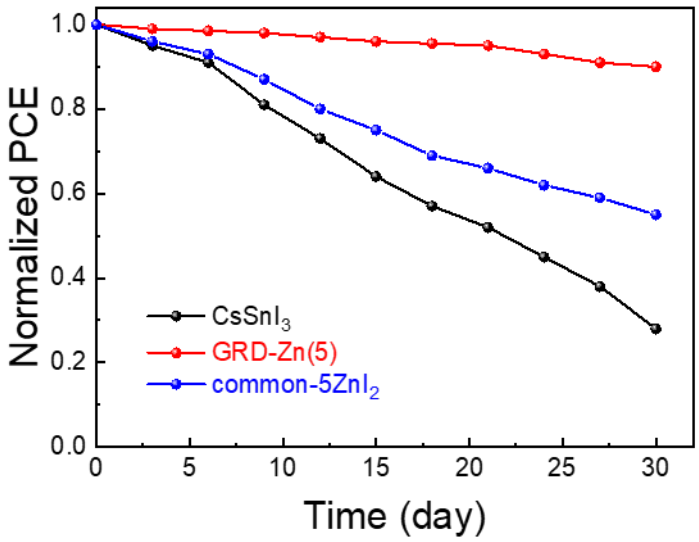

Figure S13. Time evolution of normalized PCE of the PSCs stored in the Argon-filled glovebox.

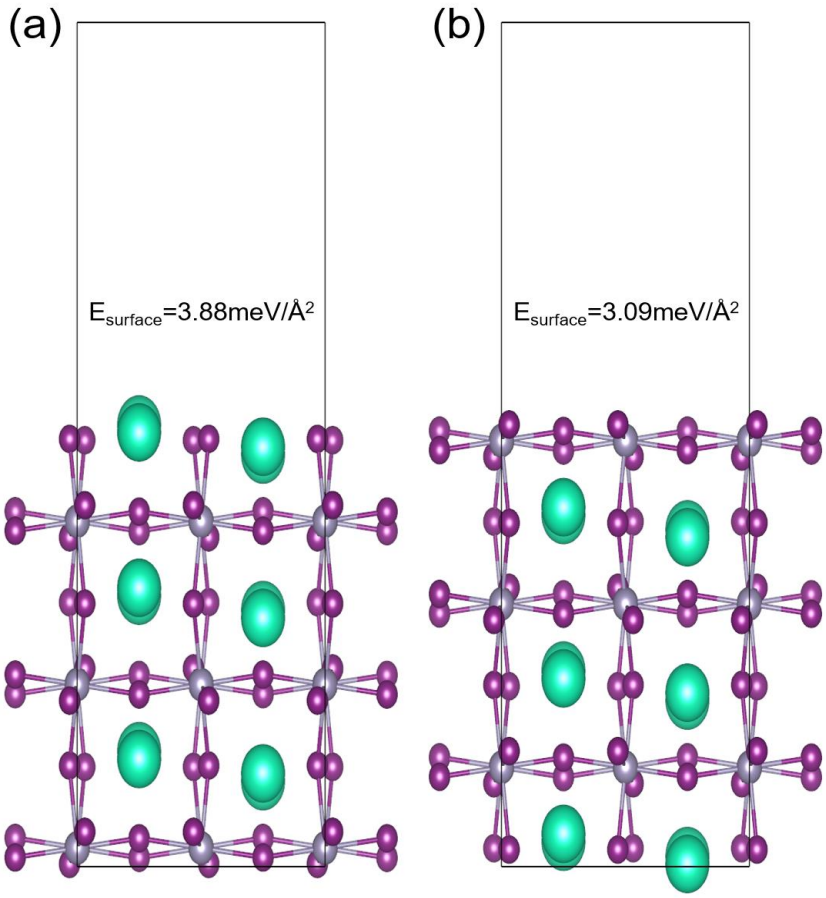

Figure S14. Schematic illustration of a) $CsSnI_3$ (202)-CsI terminal, b) $CsSnI_3$ (202)-SnI_2 terminal.

Table S1. The standard redox potentials of common divalent metal elements.

Reaction	E^0 (V)
$Ba \rightarrow Ba^{2+} + 2e^-$	2.90
$Sr \rightarrow Sr^{2+} + 2e^-$	2.89
$Ca \rightarrow Ca^{2+} + 2e^-$	2.87
$Mg \rightarrow Mg^{2+} + 2e^-$	2.37
$Mn \rightarrow Mn^{2+} + 2e^-$	1.18
$Zn \rightarrow Zn^{2+} + 2e^-$	0.76
$Cr \rightarrow Cr^{2+} + 2e^-$	0.74
$Fe \rightarrow Fe^{2+} + 2e^-$	0.44
$Cd \rightarrow Cd^{2+} + 2e^-$	0.40
$Co \rightarrow Co^{2+} + 2e^-$	0.28
$Pb \rightarrow Pb^{2+} + 2e^-$	0.13
$Sn^{2+} \rightarrow Sn^{4+} + 2e^-$	-0.15

Table S2. The detailed parameters of GDR-Zn precursor with different reaction time measured through inductively coupled plasma optical emission spectroscopy (ICP-OES).

Reaction time [h]	constant volume [ml]	Measured element	Concentration [ppm]	molar proportion [%]
0	20	Zn	0	0
	20	Sn	75.11	100
1	20	Zn	1.06	2.62
	20	Sn	72.04	97.38
2	20	Zn	1.72	4.03
	20	Sn	74.45	95.97
3	20	Zn	1.95	4.64
	20	Sn	73.37	95.36
4	20	Zn	2.08	4.98
	20	Sn	72.76	95.02
5	20	Zn	2.16	5.03
	20	Sn	74.06	94.97
6	20	Zn	2.17	5.09
	20	Sn	73.62	94.91

Table S3. The detailed parameters of GDR-Zn precursor with different reaction time measured through X-ray photoelectron spectroscopy (XPS).

Reaction time [h]	Chemical state	Peak Area [counts]	molar proportion [%]
0	Sn^{2+}	2672	5.03
	Sn^{4+}	50458	94.97
1	Sn^{2+}	1310	2.48
	Sn^{4+}	51548	97.52
2	Sn^{2+}	528	1.04
	Sn^{4+}	50214	98.96
3	Sn^{2+}	186	0.36
	Sn^{4+}	51456	99.64
4	Sn^{2+}	10	0.02
	Sn^{4+}	50148	99.98
5	Sn^{2+}	5.02	0.01
	Sn^{4+}	50234	99.99
6	Sn^{2+}	5.07	0.01
	Sn^{4+}	50697	99.99

Table S4. Detailed photovoltaic parameters of GDR-Zn (5) and control $CsSnI_3$ PSCs under different scan directions.

Device	Scan direction	V_{OC} [V]	J_{SC} [mA cm^{-2}]	FF [%]	PCE [%]
$CsSnI_3$-RS	average	0.35 ± 0.09	15.84 ± 2.88	55 ± 4.90	3.08 ± 1.85
	champion	0.44	18.72	59.80	4.93
$CsSnI_3$-FS	average	0.32 ± 0.09	15.53 ± 2.21	54 ± 5.40	2.68 ± 1.61
	champion	0.41	17.74	59.00	4.29
GDR-Zn (5)-RS	average	0.50 ± 0.02	21.83 ± 1.16	66.78 ±2.7	7.38 ± 0.89
	champion	0.52	22.93	69.40	8.27
GDR-Zn (5)-FS	average	0.48 ± 0.03	21.34 ± 1.40	64.55 ± 3.8	6.86 ± 1.11
	champion	0.51	22.74	68.70	7.97

a) RS: reverse scan; FS: forward scan.

b) The hysteresis index (HI) can be calculated by the following equation.

$$HI = [J_{RS}(0.8V_{OC}) - J_{FS}(0.8V_{OC})]/J_{RS}(0.8V_{OC})$$

where $J_{RS}(0.8V_{OC})$ and $J_{FS}(0.8V_{OC})$ on behalf of the J_{SC} at 80% of V_{OC} for the RS and FS, respectively.

Table S5. Photovoltaic performance and device structure of fully inorganic tin-based mesoporous solar cells.

Perovskite	Device structure	V_{OC} [V]	J_{SC} [mA cm^{-2}]	FF [%]	PCE [%]
$CsSnI_3$	FTO/compact TiO_2/mesoporous TiO_2/$CsSnI_3$/m-MTDATA/Au	0.24	22.70	37.0	2.02
$CsSnBr_3$	FTO/d-TiO_2/ mesoporous TiO_2/$CsSnBr_3$/spiro-MEOTAD/Au	0.42	9.10	57.0	2.17
$CsSnBr_3$	FTO/c-TiO_2/m-TiO_2/ $CsSnBr_3$/PTTA/Au	0.37	13.96	59.4	3.04
$CsSnI_3$	FTO/c-TiO_2/m-TiO_2/{en}$CsSnI_3$/PTAA/Au	0.97	18.75	24.8	3.79
$CsSnI_3$	FTO/c-TiO_2/m-TiO_2/ $CsSnI_3$/PTTA/Au	0.34	20.63	54.2	3.83
$CsSnI_3$	FTO/c-TiO_2/m-TiO_2/Al_2O_3/NiO/carbon framework	0.40	21.7	59.0	5.12
$CsSnI_3$	FTO/compact TiO_2/mesoporous TiO_2/$CsSnI_3$/P3HT/Au	0.45	24.85	67.0	7.50
$CsSnI_3$	FTO/compact TiO_2/mesoporous TiO_2/$CsSnI_3$/Al_2O_3/NiO/carbon	0.52	23.40	66.0	8.03
$CsSnI_3$	FTO/compact TiO_2/mesoporous TiO_2/$CsSnI_3$/Al_2O_3/NiO/carbon	0.52	22.93	69.4	8.27

Table S6. Summary of the parameters fitted from the TRPL spectra.

Sample	A_1	T_1 [ns]	A_2	T_2 [ns]	T_{avg} [ns]
control $CsSnI_3$	0.60	1.91	0.4	22.04	10.03
GDR-Zn (5)	0.56	0.43	0.44	9.05	4.18
common-ZnI_2	0.52	0.41	0.48	7.79	3.98

The effective carrier lifetimes (τ) were calculated by fitting with a double-exponential decay equation.

$$Y = A_1 exp\left(\frac{-t}{\tau_1}\right) + A_2 exp\left(\frac{-t}{\tau_2}\right)$$

in which, the shorter τ_1 indicates the surface recombination carrier lifetimes, while the longer τ_2 represents bulk recombination carrier lifetimes. The average PL decay lifetime were calculated by the weighted average method as follows: $\tau = (A_1\tau_1 + A_2\tau_2)/(A_1+A_2)$.

Table S7. The adsorption energy for a H_2O or O_2 molecule on perfect $CsSnI_3$ (202) surface.

Adsorbed molecule	Adsorbed Site	E_{ads} [eV]
H_2O	I-Top	-0.461
	Sn-Top	-0.781
	Bridge	-0.454
	Hollow	-0.425
O_2	I-Top	-0.156
	Sn-Top	-0.278
	Bridge	-0.119
	Hollow	-0.326

Table S8. The adsorption energy for a H_2O or O_2 molecule on Zn-substituted $CsSnI_3$ (202) surface.

Adsorbed molecule	Adsorbed Site	E_{ads} [eV]
H_2O	I-Top	-0.474
	Zn-Top	-0.541
	Bridge	-0.421
	Hollow	-0.423
O_2	I-Top	-0.096
	Zn-Top	-0.228
	Bridge	-0.109
	Hollow	-0.286

References

[1] M. Kumar, S. Dharani, W. Leong, P. Boix, R. Prabhakar, T. Baikie, C. Shi, H. Ding, R. Ramesh, M. Asta, M. Graetzel and S. Mhaisalkar, N. Mathews, *Adv. Mater*. 2014, **26**, 7122-7127.

[2] S. Gupta, T. Bendikov, G. Hodes and D. Cahen, *ACS Energy Lett.* 2016, **1**, 1028-1033.

[3] T. Song, T. Yokoyama, C. Stoumpos, J. Logsdon, D. Cao, M. Wasielewski, S. Aramaki and M. Kanatzidis, *J. Am. Chem. Soc*. 2017, **139**, 836-842.

[4] W. Ke, C. Stoumpos, I. Spanopoulos, L. Mao, M. Chen, M. Wasielewski and M. Kanatzidis, *J. Am. Chem. Soc.* 2017, **139**, 14800-14806.

[5] T. Song, T. Yokoyama, J. Logsdon, M. Wasielewski, S. Aramaki and M. Kanatzidis, *ACS Appl. Energy Mater*. 2018, **1**, 4221-4226.

[6] H. Ban, T. Zhang, X. Gong, Q. Sun, X. Zhang, N. Pootrakulchote, Y. Shen and M. Wang, *Solar RRL* 2021, **5**, 2100069.

[7] T. Ye, K. Wang, Y. Hou, D. Yang, N. Smith, B. Magill, J. Yoon, R. Mudiyanselage, G. Khodaparast, K. Wang and S. Priya, *J. Am. Chem. Soc.* 2021, **143**, 4319-4328.

[8] H. Ban, T. Nakajima, Z. Liu, H. Yu, Q. Sun, L. Dai, Y. Shen, X. Zhang, J. Zhu, P. Chene and M. Wang, *J. Mater. Chem. A* 2022, **10**, 3642-3649.